Nonlinear Optical Response of Endohedral All-Metal Electride Cages $2e^{-}Mg^{2+}(M@E_{12})^{2-}Ca^{2+}$ (M = Ni, Pd, and Pt; E= Ge, Sn, and Pb)

Hui-Min He,[a,b] Josep M. Luis,*[,b] Wei-Hong Chen,[a] Dan Yu,[a] Ying Li,[a] Di Wu,*[,a] Wei-Ming Sun,[c] and Zhi-Ru Li*[,a]

[a] *Laboratory of Theoretical and Computational Chemistry, Institute of Theoretical Chemistry, Jilin University, Changchun, 130023,China*

[b] *Institute of Computational Chemistry and Catalysis and Department of Chemistry, University of Girona, Campus de Montilivi, 17071 Girona, Catalonia, Spain*

[c] *Department of Basic Chemistry, Faculty of Pharmacy, Fujian Medical University, Fuzhou, Fujian 350108, P R China*

Abstract:

To extend the interesting new concept of all-metal electride, a series of endohedral all-metal electride cages $2e^{-}Mg^{2+}(M@E_{12})^{2-}Ca^{2+}$ (E= Ge, Sn, and Pb; M = Ni, Pd, and Pt) have been designed and investigated theoretically using exchange-correlation functional CAM-B3LYP. In these electride cage molecules with excess electrons, interesting pull-push electron transfer relay occurs. The metal cage $M@E_{12}$ first pulls valence electrons from Ca atom forming polyanion $(M@E_{12})^{2-}$, and then the formed polyanion pushes valence electrons of Mg atom out its valence shell generating the isolated excess electrons that characterize this species as all-metal electrides. These endohedral all-metal electride cages display large electronic first hyperpolarizabilities (β_0^e) and then they could have a potential application as new kind of second-order nonlinear optical (NLO) material. We have explored the structure-property relationships, which are significant. It is shown that, for a given central atom, the all-metal electrides with a Sn-cage correspond to the largest β_0^e, whereas, for a given metal cage, the all-metal electrides with Ni as central atom correspond to the largest β_0^e. Owing to the two effects, the endohedral all-metal electride cage $2e^{-}Mg^{2+}(Ni@Sn_{12})^{2-}Ca^{2+}$ exhibits the largest β_0^e value (16893 au). The same conclusions are also valid for the frequency-dependent $\beta^e(-2\omega; \omega, \omega)$ and $\beta^e(-\omega; \omega, 0)$. Moreover, we have also explored the role of the vibrational contribution on the largest components (in *x*-axis) of static β for endohedral all-metal electride cages. The vibrational contributions are significant for new all-metal electride NLO properties and therefore should be considered in the design of new NLO all-metal electrides.

1. Introduction

Designing and synthesizing novel materials with superior nonlinear optical (NLO) properties have attracted considerable interest in the light of their widespread applications in dynamic image processing, optical computing, optical switching, optical communication, optical logic, and among several others.[1-11] Electrides can serve as a kind of new nonlinear optical (NLO) molecule in which isolated excess electrons act as anions.[12] Previous studies[13, 14] have shown that introducing excess electron(s) into a molecule can markedly strengthen the static electric first hyperpolarizability (β_0). For example, by doping different kinds of organic complexants with alkali metal atoms[6, 15-20] many electride molecules with large β_0^e values were designed. Soon afterwards, a series of new strategies have been put forward to enhance the NLO response and stability of the electride molecules, including modeling how the excess electrons are pushed or pulled, size, shape, the number of coordination sites of complexants,[21] and manipulating the number and spin state of excess electron.[22] Recently, a new approach to unambiguously characterize molecular electrides based on the analysis of their electron density was reported.[23] Therefore, the design of electride molecules has entered a flourishing era.

In 2016, our group proposed the new concept "all-metal electride" inspired in the polar intermetallic compounds with Zintl polyanions.[24] Experimental and theoretical studies have shown that all-metal extended Zintl polyanions[25-29] are capable of pushing the valence electrons of an electron donor to form excess electrons. On the basis of the new concept "all-metal electride", we designed and investigated all-metal electride NLO molecules $CuAg@Ca_7M$ (M = Be, Mg and Ca).[24] In these molecules, alkaline-earth-metal atom Ca serves as the electron donor, and extended Zintl polyanions $[Cu–Ag–Be/Mg]^{4–}$ and $[Cu–Ag]^{4–}$ act as complexants pushing the remainder valence electrons of Ca atoms. We found that $[(Ca^{2+})_7(CuAgMg)^{4–}] + 10e^–$ has a large β_0^e value of 1.43×10^4 au. In addition, we theoretically designed all-metal NLO switches, i.e. all-metal electrides $M(Ni@Pb_{12})M$ (M = Be, Mg and Ca) as novel external electric field driven NLO switches.[30] Moreover, we also constructed

one-dimensional all-metal electride chains $[(Ni@Ge_9)Ca_3]_n$ (1, 2, 3, and 4) and explored their structures and electric properties.[31] In this all-metal electride multicage chain series, β_0^e increases strongly from 9321 (n = 1, N_e = 2) to 54232 au (n = N_e = 4), showing a significant cage number and excess electron number effects on the NLO response of the chains.

As explained above, we have studied the interesting effect of all-metal complexant size (i.e. metal cage number) on NLO properties. Then, a logical question to deeply understand these types of NLO molecules is: What is the effect of atomic number of all-metal complexant on NLO response? Constructing a series of endohedral all-metal electride cages with same molecular shape and exploring their property dependency on the atomic numbers of the cage atoms and central atom may be a meaningful approach to answer this question. The electronic structures of the $(M@Pb_{12})^{2-}$ (M=Ni, Pd, and Pt) icosahedral cages are unusual because the five d-orbitals of the centered transition metal give rise to a highly delocalized, three-dimensional δ-bonding orbitals.[32] Therefore, $(M@Pb_{12})^{2-}$ (M=Ni, Pd, and Pt) icosahedral cages not only have a beautiful shape and an all-metal composition, but also have pushing electron features due their two negative charges, and then it can be the basis for designing the cage of endohedral all-metal electrides.

In present work, we have designed a series of endohedral all-metal electride $Mg(M@E_{12})Ca$ (M = Ni, Pd, and Pt; E = Ge, Sn, and Pb). In this clusters the central atom M is encapsulated by E_{12} cage, and alkaline-earth metal Mg and Ca atoms sandwich the endohedral all-metal cage $M@E_{12}$, which act as electron acceptor. Considering functions of alkaline-earth metals, the Ca atom serves as the electron source to form endohedral all-metal Zintl cage polyanions $(M@E_{12})^{2-}$ and Mg atom serves as the excess electron source in the interesting intramolecular pull-push electron transfer relay. In this work, we show that the studied all-metal electrides exhibit large first hyperpolarizabilities of endohedral all-metal electride cages, reveal the effects of the atomic number of cage and encapsulated central atoms on their NLO properties, find new strategies for enhancing their first hyperpolarizabilities, and propose new endohedral all-metal electrides which may be used as NLO materials.

2. Computational Methods

For NLO calculations, it has been reported that the values of first hyperpolarizability (β_0) are quite sensitive to the basis set used.[33-38] Zalesny and his coworkers have found CAM-B3LYP is a successful DFT method for calculating hyperpolarizabilities of large system.[39] Then the calculations of equilibrium geometries and corresponding properties of all-metal electride cage molecules Mg(M@E_{12})Ca (E = Ge, Sn, and Pb; M = Ni, Pd, and Pt) with all real frequencies have been performed using the CAM-B3LYP functional.[40, 41] The Pople-type basis sets[42] 6-311+G* for Mg and Ca, and Los Alamos double-zeta type set[43-45] LANL2DZ+diffuse function for Ni, Pd, Pt, Ge, Sn, and Pb are selected.

The vertical ionization potential (VIP) is calculated at same level. The VIP is noted as follows:[18]

VIP = $E[M^+]$ - $E[M]$

where the energies $E[M^+]$ and $E[M]$ are calculated at the optimum geometry of the neutral molecule. For electronic transition properties, the transition energy ΔE, oscillator strength f_0, and the difference of dipole moment $\Delta\mu$ between the ground and the crucial excited state are estimated by TD-CAM-B3LYP/6-311+G*/LANL2DZ+diffuse function.

The static electronic first hyperpolarizability (β_0^e) is noted as follows:

$$\beta_0^e = (\beta_x^2 + \beta_y^2 + \beta_z^2)^{1/2}$$

where

$$\beta_i = \frac{3}{5}\sum_{j=x,y,z}\beta_{ijj}$$

For the longitudinal component of vibrational (nuclear relaxation) first hyperpolarizability (β_{xxx}^{nr}), we use the numerical finite field NR (i.e., FF-NR) methodology.[46] In the FF-NR methodology, one needs to optimize the geometry in the presence of a finite static field while strictly imposing the Eckart conditions.[47] Then, a finite field numerical differentiation of the electronic energy is carried out, in this paper using field strengths of ±0.0002, ±0.0004, ±0.0008, ±0.0016, ±0.0032, and ±0.0064 au. The smallest magnitude field that produced a stable vibrational NLO

property was selected using a Romberg method triangle.[48]

According to Bishop and co-workers,[49] if we denote the equilibrium molecular geometry with a static electric field F present by R_F and without the field present, by R_0, then we may define:

$$(\Delta\mu_i^e)_{R_0} = \mu_i^e(\mathrm{F},R_0) - \mu_i^e(0,R_0) \quad (1)$$

and $$(\Delta\mu_i^e)_{R_F} = \mu_i^e(\mathrm{F},R_F) - \mu_i^e(0,R_0) \quad (2)$$

The electronic contribution to the (hyper)polarizabilities can be derived from the expansion of Eq. (1). But the expansion of Eq. (2) leads to the definition of the electronic and also the vibrational (nuclear relaxation) contributions to the (hyper)polarizabilities,

$$\mu_i^e(F, R_F) = a_1F_j + 1/2b_1F_jF_k + \cdots \quad (3)$$

where

$$a_1 = \alpha_{ij}^e(0;0) + \alpha_{ij}^{nr}(0;0) + \cdots \quad (4)$$

$$b_1 = \beta_{ijk}^e(0;0,0) + \beta_{ijk}^{nr}(0;0,0) + \cdots \quad (5)$$

β^e and β^{nr} denote the electronic and vibrational (nuclear relaxation) contributions to the (hyper)polarizabilities.[50]

The frequency-dependent first hyperpolarizabilities of these all-metal electride cages were obtained by the coupled perturbed Hartree-Fock (CPHF) method.[51, 52] The basis set employed are the LANL2DZ+diffuse function for Ni, Pd, Pt, Ge, Sn, and Pb and 6-311+G* for Mg and Ca. The frequency-dependent is noted as[53]

$$\beta^e(\omega) = (\beta_x^2 + \beta_y^2 + \beta_z^2)^{1/2}$$

Where

$$\beta_i = \frac{1}{5}[2\beta_{jji}(-2\omega;\omega,\omega) + \beta_{ijj}(-2\omega;\omega,\omega)] \text{ (i, j = x, y, and z)}$$

for the second-harmonic generation (SHG) and

$$\beta_i = \frac{1}{5}\sum_{j=x,y,z}[\beta_{jji}(-\omega;\omega,0) + 2\beta_{jij}(-\omega;\omega,0)]$$

for the electro-optical Pockels effect (EOPE).

All of the calculations were carried out using the Gaussian09 program package.[54] Molecular orbitals were visualized with the GaussView program.[55]

3. Results and discussion

3.1 Equilibrium geometries, electride features, and molecular stabilities

The ground state optimized structures with all real frequencies of the nine endohedral all-metal cages Mg(M@E_{12})Ca (E = Ge, Sn, and Pb; M = Ni, Pd, and Pt) are given in Figure 1. Figure 1 shows that these structures possesses a same structural mode in which alkaline-earth metal Mg and Ca atoms sandwich the endohedral all-metal cage M@E_{12}. Selected geometrical parameters of these studied endohedral all-metal cages are summarized in Table 1. As shown in Table 1, for a set of molecular structures Mg(M@E_{12})Ca (E = Ge, Sn, and Pb) with a given M, the distance Mg−Ca increases along with the increasing atomic number of metal E, that is, the larger the atomic number of E, the longer the Mg−Ca distance, exhibiting a correlation with the atomic radius of E. The same general trend is also valid for the smallest Ca-E bond distance.

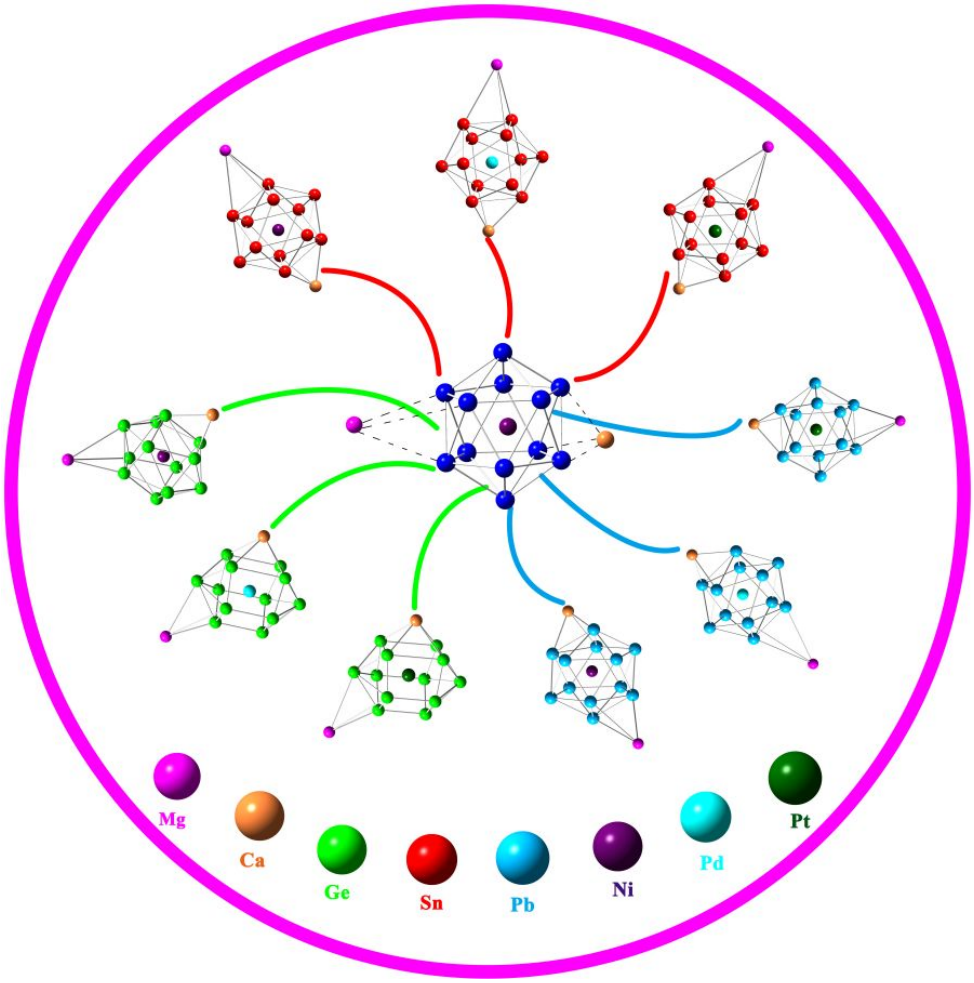

Figure 1 Geometric structure of Mg(M@E_{12})Ca (M = Ni, Pd, and Pt; E = Ge, Sn, and Pb) All-Metal Electride cages.

Table 1 Selected Geometric Parameters (in Å) including Mg-Ca distance, the smallest Mg-E distance, the smallest Ca-E distance and $\angle_{Mg\text{-}M\text{-}Ca}$. First Vertical Ionization potentials (VIP, in eV) and HOMO−LUMO Gaps (H−L Gap, in eV) of endohedral all-metal electride cages $Mg(M@E_{12})Ca$ (M = Ni, Pd, and Pt; E= Ge, Sn, and Pb). Atomic Radius R(A) (in Å).

	Mg-Ca	Mg-E	Ca-E	$\angle_{Mg\text{-}M\text{-}Ca}$	VIP	H-L Gap	R(A)
$Mg(Ni@Ge_{12})Ca$	9.06	3.56	2.85	130	6.56	3.48	1.25(Ge)
$Mg(Ni@Sn_{12})Ca$	10.62	4.29	3.06	180	5.93	3.31	1.45(Sn)
$Mg(Ni@Pb_{12})Ca$	10.91	4.26	3.08	164	5.72	3.19	1.80(Pb)
$Mg(Pd@Ge_{12})Ca$	8.61	3.15	2.94	132	6.13	3.70	1.35(Ni)
$Mg(Pd@Sn_{12})Ca$	10.81	4.44	3.06	180	6.05	3.35	1.40(Pd)
$Mg(Pd@Pb_{12})Ca$	11.05	4.35	3.09	164	5.70	3.23	1.35(Pt)
$Mg(Pt@Ge_{12})Ca$	8.69	3.26	2.93	133	6.15	3.82	
$Mg(Pt@Sn_{12})Ca$	10.82	4.53	3.07	180	5.89	3.39	1.50(Mg)
$Mg(Pt@Pb_{12})Ca$	11.08	4.43	3.09	163	5.64	3.24	1.80(Ca)

However, the smallest Mg−E distance present its maximum for E=Sn. From table 1, we can also find that these three electrides with E=Ge has optimum geometries clearly different from the other six all-metal electrides. The values of its smallest Mg-Ge distances are only in the range of 3.15-3.56 Å. Furthermore, due to a skewing of Mg out of Ca-M axis, their Mg-Ca distances are only in the range of 8.61-9.06Å. We also note that in these six electrides with E = Sn and Pb, the Mg-M-Ca angle is about 180º, but its value for $Mg(M@Ge_{12})Ca$ is about 130°, which results from skewing of Mg out of Ca-M axis. Besides, It is interesting to note that the Mg−E distance are larger than the corresponding Ca−E distance values, which is in disagreement with the corresponding sum of atomic radius.

In each all-metal cage, an interesting pull−push electron transfer relay occurs. All-metal cage $M@E_{12}$ pull valence electrons from the electron source-alkaline-earth metal Ca atom and becomes an electron pushing complexant, namely, all-metal Zintl polyanion $(M@E_{12})^{2-}$. Then, the polyanion $(M@E_{12})^{2-}$ pushes the two valence electrons of the excess electron source-Mg atom forming two excess electrons located close to Mg^{2+}. Thus, the electronic structure of the endohedral all-metal cage is represented as $2e^{-}Mg^{2+}(M@E_{12})^{2-}Ca^{2+}$ and it may be proposed as an endohedral all-metal electride cage with two isolated excess electrons. The HOMOs of these

endohedral all-metal cages depicted in Figure 2 indicate the presence of excess electron close to Mg, which supports the conclusion that the endohedral all-metal cages are endohedral all-metal electride cages.

Taking into account the existence of loosely bound excess electrons, it is relevant to investigate the electronic stability of these all-metal electride cage molecules. The electronic stability of a molecule may be characterized by its first vertical ionization potential (VIP) value. The VIPs of $2e^{-}Mg^{2+}(M@E_{12})^{2-}Ca^{2+}$ (M = Ni, Pd, and Pt; E = Ge, Sn, and Pb) are in the range of 5.64-6.29 eV (see Table 1). The VIP values decrease with the atomic number of the cage atoms, whereas M atomic number effect on VIP is small. The VIP correlates with the size of the spherical lobe rounding Mg in HOMO, which is associated to the dispersion of excess electron density. The VIP values of these molecules are slightly larger than the reported values of inorganic, organic and other all-metal electride molecules,[15, 24, 30, 31, 56] but smaller than the very larger value (7.78 eV) of the electride molecule with the excess electron protected inside the $C_{36}F_{36}$ cage.[57] Hence, these all-metal electride cages exhibit larger electronic stability than most of the investigated electride molecules.

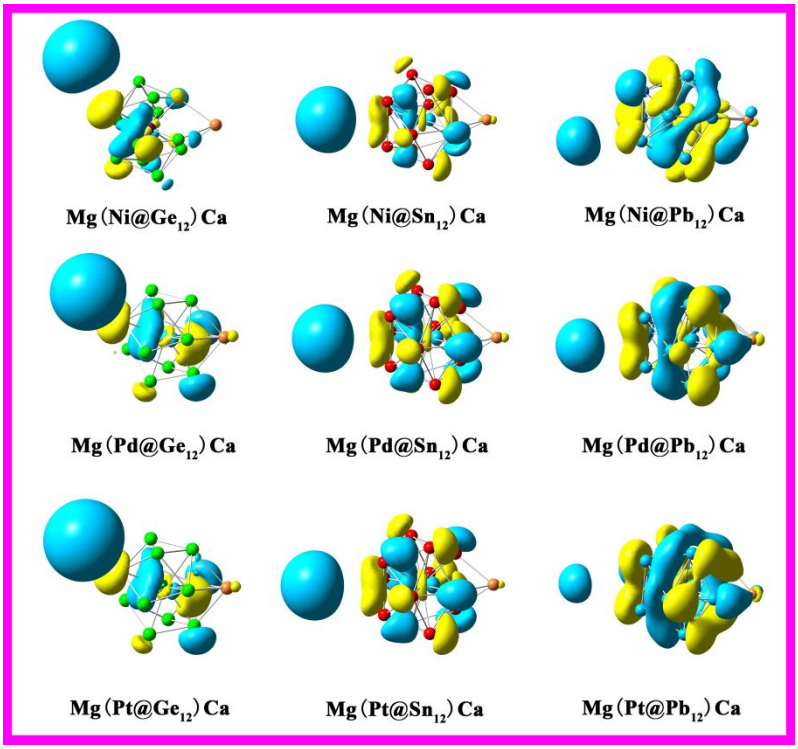

Figure 2 The HOMO isosurfaces of $2e^{-}Mg^{2+}(M@E_{12})^{2-}Ca^{2+}$ (M = Ni, Pd, and Pt; E = Ge, Sn, and Pb).

Table 2 Transition energies (ΔE, in eV), oscillator strengths (f_0), and difference of dipole moment ($\Delta\mu$, in D) between the ground and the crucial excited state, static electronic first hyperpolarizability β_0^e, and crucial transitions for Mg(M@E_{12})Ca (M = Ni, Pd, and Pt; E = Ge, Sn, and Pb).

	ΔE	$\Delta\mu$	f_0	$\Delta\mu f_0/\Delta E^3$	β_0^e	Crucial transtion
Mg(Ni@Ge_{12})Ca	2.99	11.39	0.1474	496	7503	72% H-6→L
Mg(Ni@Sn_{12})Ca	2.29	14.31	0.3159	2984	16893	56% H-5→L
Mg(Ni@Pb_{12})Ca	2.09	6.98	0.1851	1117	14151	63% H-5→L
Mg(Pd@Ge_{12})Ca	2.48	6.03	0.1474	529	5098	50% H→L+3
Mg(Pd@Sn_{12})Ca	2.32	12.15	0.2458	1889	14206	63% H-5→L
Mg(Pd@Pb_{12})Ca	2.11	4.02	0.0838	286	12677	41% H-5→L
Mg(Pt@Ge_{12})Ca	2.58	9.72	0.1106	496	4848	61% H→L+3
Mg(Pt@Sn_{12})Ca	2.37	11.66	0.2354	1632	11895	61% H-5→L
Mg(Pt@Pb_{12})Ca	2.11	7.10	0.1626	974	11386	72% H-5→L

It is well-known that the gap between the HOMO (highest occupied molecular orbital) and LUMO (lowest unoccupied molecular orbital) is another useful quantity for examining the molecular chemical stability. A large gap value reflects a high chemical stability. Table 1 lists HOMO−LUMO (H−L) gaps of these all-metal electride cages $2e^-Mg^{2+}(M@E_{12})^{2-}Ca^{2+}$ (M = Ni, Pd, and Pt; E = Ge, Sn, and Pb), which are in the range of 3.19-3.82 eV. These HOMO−LUMO gap values are comparable or larger than the HOMO-LUMO gap value of about 3.5 eV of the $CuAg@Ca_7M$ (M = Be, Mg and Ca) all-metal electride molecules.[24] Therefore, $2e^-Mg^{2+}(M@E_{12})^{2-}Ca^{2+}$ (M = Ni, Pd, and Pt; E = Ge, Sn, and Pb) have chemical stabilities close to other all-metal electrides.

3.2 First hyperpolarizabilities

3.2.1. Static electronic and vibrational first hyperpolarizabilities.

Now, we focus on the effect of atomic number of the cage and the encapsulated central atoms on the molecular static first hyperpolarizabilities. The calculated static first electronic hyperpolarizabilities for all-metal electride cage molecules are exhibited in Table 2 and Figure 3. These values of β_0^e are in the range of 4848-16893 au. These endohedral all-metal electride cages with excess electrons display large first hyperpolarizabilities (β_0^e), thus they may be considered as a new class of endohedral all-metal electride cage NLO molecules.

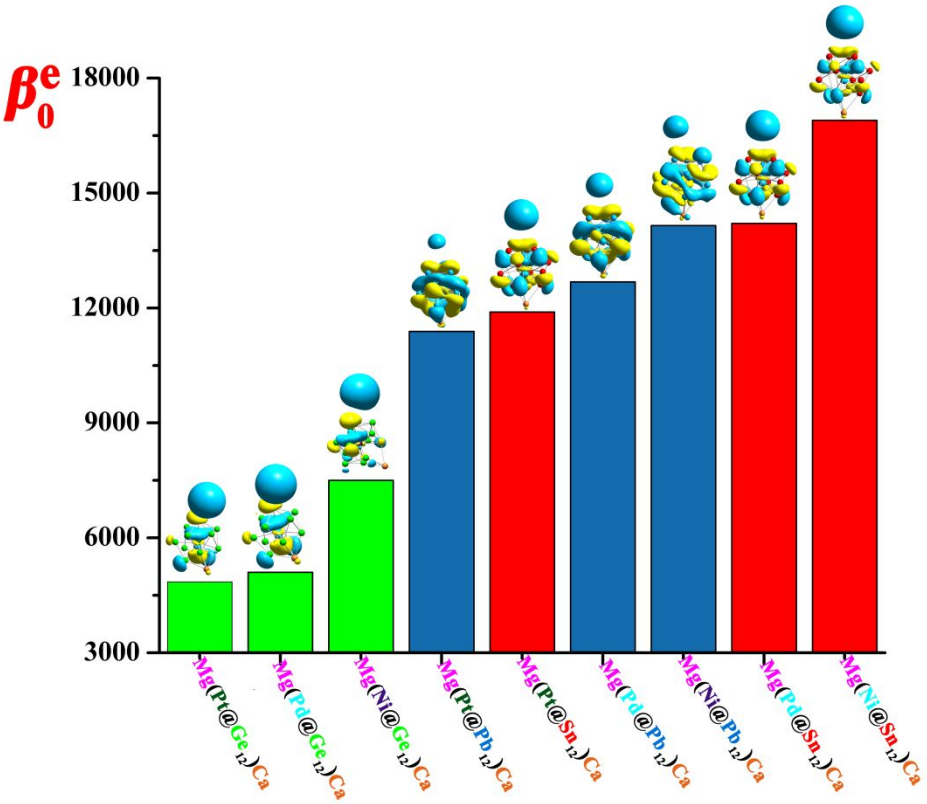

Figure 3 β_0^e of $2e\text{-}Mg^{2+}(M@E_{12})^{2-}Ca^{2+}$ (E = M = Ni, Pd, and Pt; Ge, Sn, and Pb).

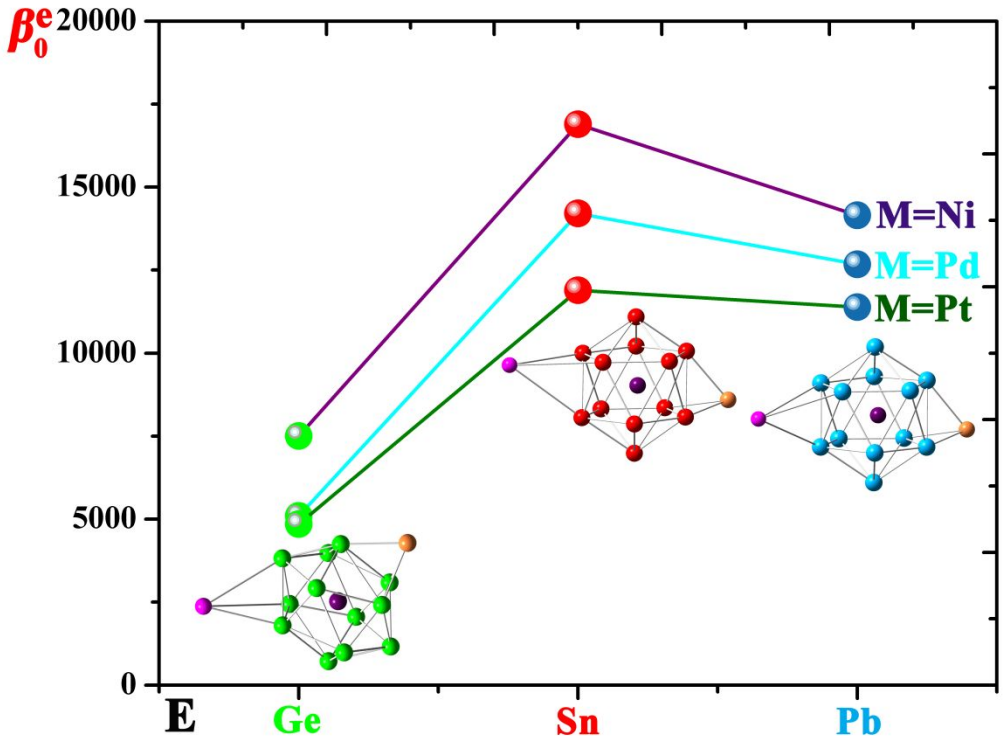

Figure 4 The effect of the atomic number of cage atoms (E, color balls) and encapsulated central atom (M, color lines) on β_0^e.

The relationship between the β_0^e value and the atomic number of cage atoms (E) for all-metal electride cage NLO molecules can be presented by a mono-peak curve, as shown in Figure 4. The maximum values of β_0^e correspond to E=Sn, are 16893(M=Ni), 14206 (M=Pd) and 11895 (M=Pt) au. Therefore, the selection of Sn cages is an effective strategy for enhancing the first hyperpolarizability of all-metal electride cage NLO molecules.

For a given E_{12} cage, the β_0^e value decrease when atomic number M increases (see Figure 4), namely for E = Ge, 9583 (M=Ni) > 6780 (M=Pd) > 4848 au (M=Pt); for E = Sn 16893 (M=Ni) > 14206 (M=Pd) > 11895 au (M=Pt); and for E = Pb 14151(M=Ni) > 12677 (M=Pd) > 11386 (M=Pt). This results shows that the use of M=Ni leads to the largest β_0^e for the all-metal electride cage molecule $2e^-Mg^{2+}(M@E_{12})^{2-}Ca^{2+}$.

Based on preceding discussions, the two strategies for enhancing β_0^e consist one selecting Ni as central atom and Sn as cage atoms, leading to all-metal electride cage molecule $2e^-$ $Mg^{2+}(Ni@Sn_{12})^{2-}Ca^{2+}$, which have the largest β_0^e value (16893 au).

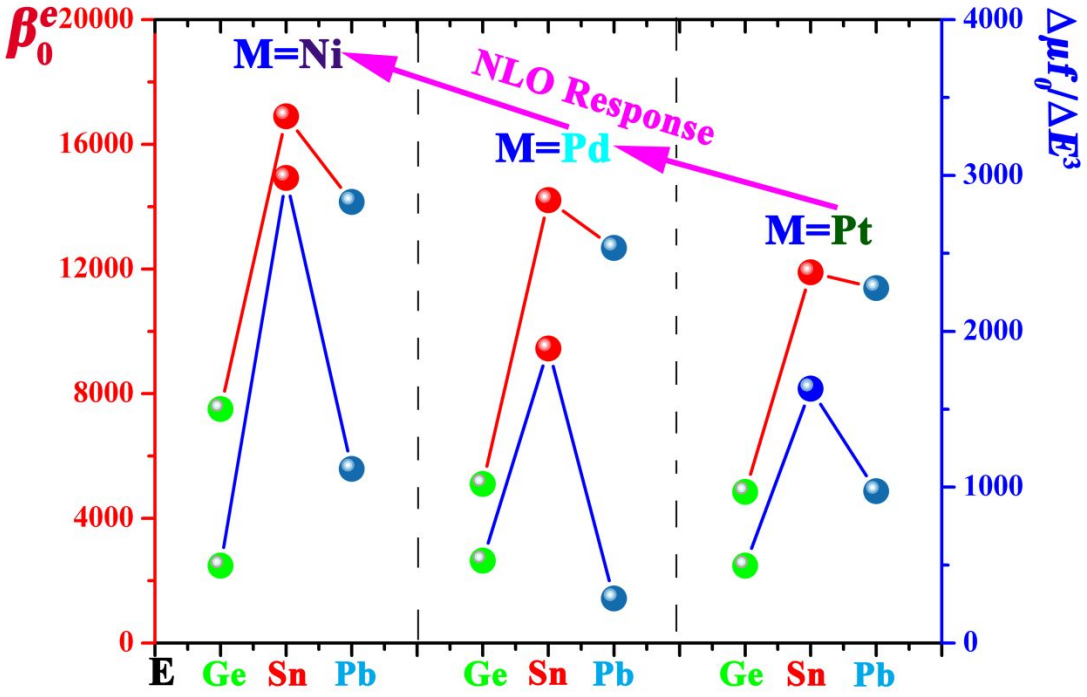

Figure 5 The relationship of β_0^e (red lines) and $\Delta\mu f/\Delta E^3$ (blue lines).

But, how can one rationalize the variations of β_0^e value of $2e^-Mg^{2+}(M@E_{12})^{2-}Ca^{2+}$ with the changing M and E atomic number? We may consider the two-level model[19, 37]

$$\beta_0 \propto \frac{\Delta\mu f_0}{\Delta E^3}$$

where ΔE, f_0, and $\Delta\mu$ are the transition energy, oscillator strength, and difference in the dipole moment between the ground state and the crucial excited state, respectively. From the two-level expression, β_0 is proportional to f_0 and $\Delta\mu$, whereas it is inversely proportional to the second power of ΔE. Herein, the crucial excited states of $2e^-Mg^{2+}(M@E_{12})^{2-}Ca^{2+}$ were obtained, and the corresponding ΔE, f_0, and $\Delta\mu$ values as well as dominate transitions are presented in Table 2. By considering two-level model, the trend of $\frac{\Delta\mu f_0}{\Delta E^3}$ evolution agrees with that of β_0^e evolution as shown in Figure 5. Therefore, in all-metal electride systems, first electronic hyperpolarizability (β_0^e) evolution trend can be easily reproduced with two-level model. The results of table 2 also show that the tree factors of two-model formula (i.e. ΔE, f_0, and $\Delta\mu$) have a key role determining the variation of β_0^e of the all-metal electride cage NLO molecules.

The β_0^e values of our new all-metal electride cages ($4848 - 16893$ au) is comparable to the values of some of previously reported electrides: 7326 for an organic electride Li@calix[4]-pyrrole,[15] 10645 for LiCNLi@BNNT,[56] 7197 for $Cup\cdots K_3O^+\cdots e@C_{36}F_{36}^-$,[57] 12782 for inorganic electride molecule $Ca\text{-}(NH_3)_6Na_2(b'')$,[58] and 14300 au for all-metal electride molecule $CuAg@Ca_7Mg(1)$.[24] Nevertheless, there are also some reported electride molecules which exhibited larger β_0^e values compared with the β_0^e of $2e^-Mg^{2+}(M@E_{12})^{2-}Ca^{2+}$. For example, the β_0^e values of new inorganic electride compound $M@r6 - Al_{12}N_{12}$,[59] $Na–(C_2NH_5)_4$[60] and $e^-@C_{20}F_{19}^-(CH_2)^{4-}NH_2\cdots Na^+$ [18] are, respectively, 8.89×10^5, 3.4×10^6 and 9.5×10^6 au.

It is well known that in addition to the electronic contribution, the effect of vibrations on the hyperpolarizabilities is also quite important.[7, 9-11] Garcia-Borràs *et*

Table 3 The largest component (in X-axis) of the Static electronic and vibrational contributions to μ, α, and β (in a.u.) for all-metal electrides $2e^{-}Mg^{2+}(M@E_{12})^{2-}Ca^{2+}$ (M = Ni, Pd, and Pt; E = Ge, Sn, and Pb). The magnitudes of the ratio between the NR and corresponding static electronic properties (*nr*/*e*) are given in italics.

	μ_x	α^{e}_{xx}	α^{nr}_{xx}	*nr/e*	β^{e}_{xxx}	β^{nr}_{xxx}	*nr/e*
Mg(Ni@Ge12)Ca	4.93	648	123	*0.18*	-9.28×10^{3}	5.30×10^{4}	*3.57*
Mg(Ni@Sn12)Ca	4.93	950	56	*0.06*	-2.71×10^{4}	1.90×10^{4}	*0.70*
Mg(Ni@Pb12)Ca	4.11	1012	76	*0.08*	-2.18×10^{4}	2.79×10^{4}	*0.13*
Mg(Pd@Ge12)Ca	3.21	674	145	*0.21*	-5.17×10^{3}	4.04×10^{4}	*3.85*
Mg(Pd@Sn12)Ca	4.88	940	58	*0.06*	-2.26×10^{4}	2.69×10^{4}	*1.19*
Mg(Pd@Pb12)Ca	3.88	997	78	*0.08*	-1.65×10^{4}	3.81×10^{4}	*2.31*
Mg(Pt@Ge12)Ca	3.29	661	114	*0.17*	-5.02×10^{3}	-4.38×10^{4}	*8.71*
Mg(Pt@Sn12)Ca	4.78	916	88	*0.10*	-1.88×10^{4}	3.32×10^{4}	*1.77*
Mg(Pt@Pb12)Ca	3.99	997	103	*0.10*	-1.73×10^{4}	4.11×10^{4}	*2.38*

al. have previously investigated the key role of the vibrational NLO properties for a representative set of electrides.[61] Their results showed that vibrational contribution can be quite important and may even be much larger than the electronic counterpart. In Table 3, we present the comparison between the electronic and vibrational contributions of α and β for the *x*-axis component of all-metal electride cages $2e^{-}Mg^{2+}(M@E_{12})^{2-}Ca^{2+}$. The ratios between the vibrational and electronic contribution are small, in the range of about 0.06-0.21, for α_{xx}. On the contrary, the nr/e ratios are quite large, in range of 1.19-8.71, for β_{xxx}, except for $2e^{-}Mg^{2+}(Ni@Pb_{12})^{2-}Ca^{2+}$ and $2e^{-}Mg^{2+}(Ni@Sn_{12})^{2-}Ca^{2+}$ which nr/e ratios are 0.13 and 0.70, respectively. Noteworthy, for $2e^{-}Mg^{2+}(Pt@Ge_{12})^{2-}Ca^{2+}$, vibrational contribution to β_{xxx} is far larger than its electronic contribution (nr/e = 8.71). Interestingly, the dependency of β^{nr}_{xxx} on the atomic numbers of E and M is different than the dependency showed by the electronic contribution. For a given M, the variation of absolute value of β^{nr}_{xxx} of $2e^{-}Mg^{2+}(M@E_{12})^{2-}Ca^{2+}$ with the atomic number of E follows the Ge > Pb > Sn order. And for a given E, absolute value of β^{nr}_{xxx} of $Mg(M@E_{12})Ca$ with E=Sn and Pb increase with the increasing atomic number of M. However, when E=Ge, the variation of absolute value of β^{nr}_{xxx} of $2e^{-}Mg^{2+}(M@E_{12})^{2-}Ca^{2+}$ is different due to a skewing of Mg. Our results clearly point that the vibrational contribution should be

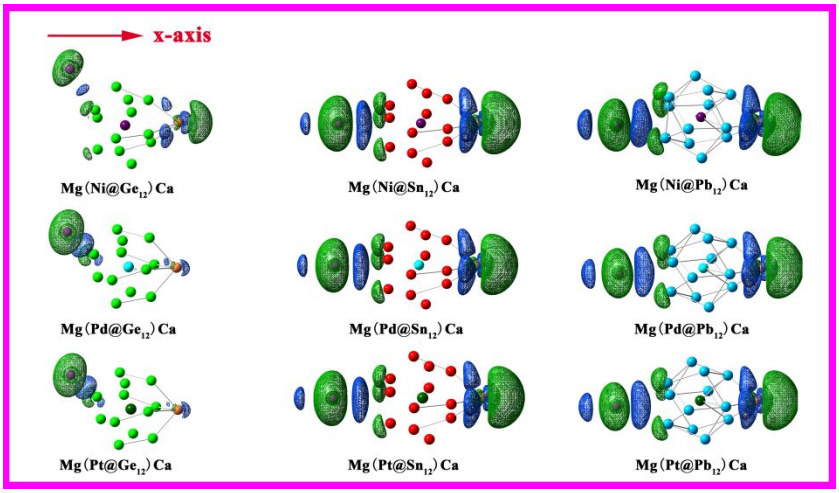

Figure 6 The diagrams of $-x^{*}\rho_{xx}^{(2)}(r)$ for $2e^{-}Mg^{2+}(M@E_{12})^{2-}Ca^{2+}$ (E = Ge, Sn, and Pb; M = Ni, Pd, and Pt), in which blue and green meshes represent the positive and negative density contributions to β_{xxx}^{e} respectively.

considered to properly determine the nonlinear optical properties of the endohedral all-metal electride cage NLO molecules.

It is noted that, the β_{xxx}^{e} values in Table 3 are negative. To rationalize the origin of this negative sign we used the so-called electronic first hyperpolarizability density. The expansion of the electron density $\rho(r, F)$ in terms of an applied external electric field F is given by:[62]

$$\rho(r,F)=\rho^{(0)}(r)+\rho^{(1)}(r)F+\frac{1}{2}\rho^{(2)}(r)F^{2}+\frac{1}{6}\rho^{(3)}(r)F^{3}+\cdots,$$

where the second-order derivative of electron density $\rho^{(2)}(r)$ is related with the electronic first hyperpolarizability β_0. In fact, β_{xxx} can be obtained by the integration of $-x\rho_{xx}^{(2)}(r)$, which can be then considered as the x diagonal component of the electronic first hyperpolarizability.[62] $\rho_{xx}^{(2)}(r)$ can be calculated at each spatial point by using the following second order numerical differentiation:

$$\rho_{xx}^{(2)}(r)=\frac{\rho(r,F_x)-2\rho(r,0)+\rho(r,-F_x)}{(F_x)^{2}}$$

The x diagonal component of first hyperpolarizability density distributions of $2e^{-}Mg^{2+}(M@E_{12})^{2-}Ca^{2+}$ are plotted in Figure 6, in which blue and green meshes represent the positive and negative contribution to β_{xxx}^{e}, respectively. It can be seen that negative contribution of green meshes around alkaline-earth- metal atoms is the

main contribution of electron density for β^e_{xxx} values, so the β^e_{xxx} values are negative. The $2e^-Mg^{2+}(Pt@Ge_{12})^{2-}Ca^{2+}$, which has the smallest β^e_{xxx} value, corresponds to the smallest green meshes around alkaline-earth-metal atoms.

3.4.2. Frequency-dependent first hyperpolarizabilities

To understand the dispersion effect on the β^e_0 value, the frequency-dependent β_e of the molecular all-metal electride cages were calculated using the CPHF method. Table 4 lists the frequency- dependent values of electro-optical Pockels effect (EOPE) $\beta^e(-\omega; \omega, 0)$ and second-harmonic generation (SHG) $\beta^e(-2\omega; \omega, \omega)$. As shown in Table 4 and Figure 7, for all-metal electride cages $2e^-Mg^{2+}(M@E_{12})^{2-}Ca^{2+}$ with E= Sn and Pb, the computed $\beta^e(-2\omega; \omega, \omega)$ and $\beta^e(-\omega; \omega, 0)$ at ω = 0.005 and 0.01 au are slightly larger than the corresponding static β^e_0 at ω = 0.0 au. However, for all-metal electride cages with E = Ge, the order is just opposite. For each all-metal electride cage, the frequency-dependent value increases with the increment of the optical frequency. For example, for $2e^-Mg^{2+}(Ni@Sn_{12})^{2-}Ca^{2+}$, the $\beta^e(-2\omega; \omega, 0)$ at ω = 0.010 is about 1.07 times larger than that at ω = 0.005 au. It is also shown that the $\beta^e(-2\omega; \omega, \omega)$ is larger than the $\beta^e(-\omega; \omega, 0)$ for each all-metal electride cage. Significantly, the frequency-dependent $\beta^e(-2\omega; \omega, \omega)$ and $\beta^e(-\omega; \omega, 0)$ at ω = 0.005 and 0.01 au show the equivalent dependence on the atomic number of the M and E atoms. Therefore, for

Table 4 Frequency-dependent $\beta^e(-2\omega; \omega, \omega)$ and $\beta^e(-\omega; \omega, 0)$ values (au) for $2e^-Mg^{2+}(M@E_{12})^{2-}Ca^{2+}$ (M = Ni, Pd, and Pt; E= Ge, Sn, and Pb) calculated at the CAM-B3LYP level.

		ω=0.005		ω=0.01	
	β^e_0	$\beta^e(-\omega;\omega,0)$	$\beta^e(-2\omega;\omega,\omega)$	$\beta^e(-\omega;\omega,0)$	$\beta^e(-2\omega;\omega,\omega)$
$Mg(Ni@Ge_{12})Ca$	7503	7147	7215	7249	7535
$Mg(Ni@Sn_{12})Ca$	16893	17132	17380	17506	18571
$Mg(Ni@Pb_{12})Ca$	14151	14597	14813	14920	15855
$Mg(Pd@Ge_{12})Ca$	5098	4037	4078	4098	4270
$Mg(Pd@Sn_{12})Ca$	14206	14432	14630	14731	15579
$Mg(Pd@Pb_{12})Ca$	12677	13064	13255	13353	14183
$Mg(Pt@Ge_{12})Ca$	4848	4509	4557	4581	4784
$Mg(Pt@Sn_{12})Ca$	11895	12088	12240	12317	12963
$Mg(Pt@Pb_{12})Ca$	11386	11793	11950	12030	12705

a given M central atom, the Sn-cage corresponds to the largest frequency dependent β^e. And again, for a given E cage atom, the frequency dependent β^e strongly increases with decreasing the atomic number of central atom M metal. For instance, for E = Sn, $\beta^e(-2\omega; \omega, \omega)$ values at ω = 0.01 au are 18571 au (M=Ni) > 15579 (M=Pd) > 12963 (M = Pt). Therefore, although external optical frequency ω changes the values of the electronic first hyperpolarizability, does not change the dependency of β^e with atomic number of cage atoms (E) and encapsulated central atom (M) for endohedral all-metal electride cages $2e^-Mg^{2+}(M@E_{12})^{2-}Ca^{2+}$ (M = Ni, Pd, and Pt; E = Ge, Sn, and Pb).

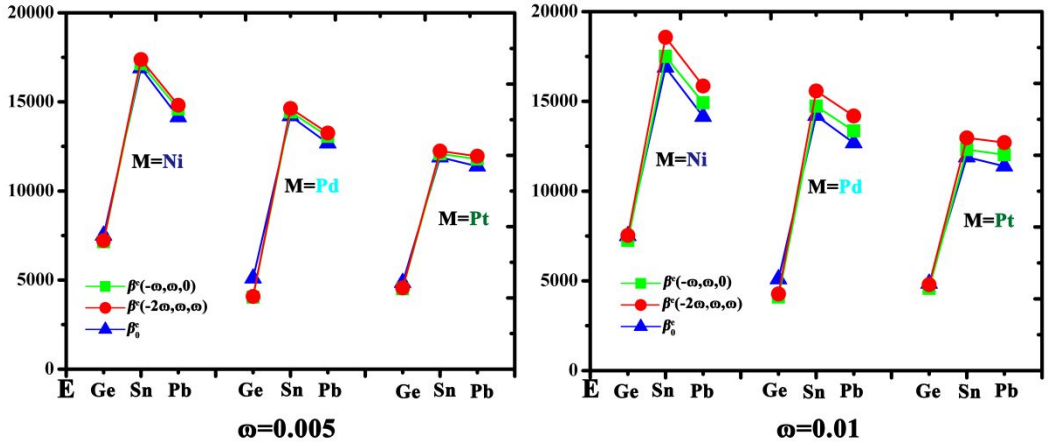

Figure 7 The frequency-dependent $\beta^e(-2\omega, \omega, \omega)$ and $\beta^e(-\omega, \omega, 0)$ values of $2e^-Mg^{2+}(M@E_{12})^{2-}Ca^{2+}$ (M = Ni, Pd, and Pt; E= Ge, Sn, and Pb) calculated at the CAM-B3LYP level at ω = 0.005 and 0.01 au.

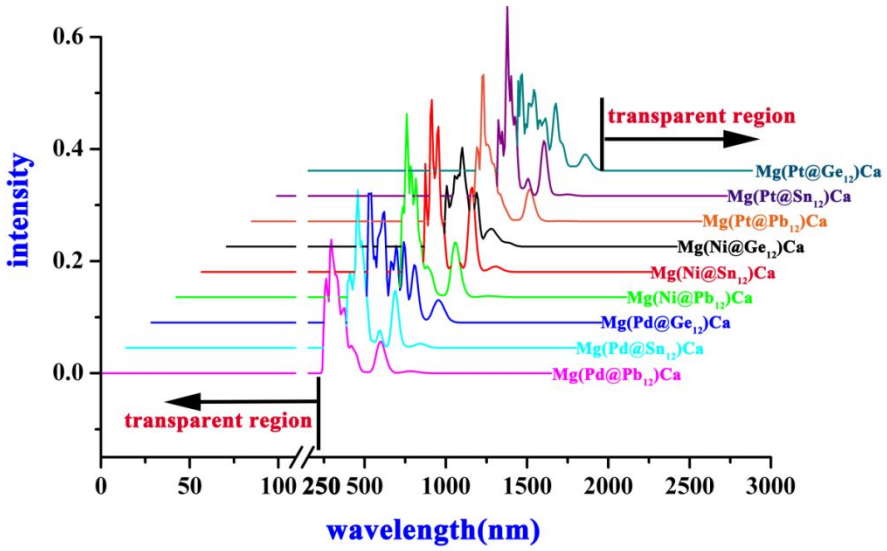

Figure 8 Electronic absorption spectra of all-metal electride cage molecules.

For the NLO molecules, the transparent region of the electronic absorption spectrum is selected as its working waveband. The region of the working waveband has great of NLO devices. Figure 8 shows that the nine all-metal electride cage molecules studied here have an infrared (IR) transparent region at wavelength > 2000 *nm*. Thus, these nine all-metal electride cage molecules could be used as new IR NLO materials. Simultaneously, they also have an ultraviolet (UV) transparent region at wavelength < 250 *nm*. Then, these all-metal electride cage molecules could be also used as new UV NLO materials.

4. Conclusions

A series of endohedral all-metal electride cages $2e^{-}Mg^{2+}(M@E_{12})^{2-}Ca^{2+}$ (M = Ni, Pd, and Pt; E= Ge, Sn, and Pb) have been designed and theoretically investigated as potential candidates for a new kind of NLO material. The molecular electride characteristics of the nine all-metal cage molecule are originated from an interesting mechanism of intramolecular pull-push electron transfer relay. The metal cage $M@E_{12}$ first pulls valence electrons from Ca atom forming polyanion $(M@E_{12})^{2-}$, and then formed polyanion pushes valence electrons of Mg atom forming isolated excess electrons. Owing to the existence of excess electrons, these endohedral all-metal electride cages display large electronic and vibrational first hyperpolarizabilities and then can be considered a new type of NLO molecule. The effects of the atomic number of cage atoms (E) and encapsulated central atom (M) on β_0^e have been revealed. It is shown that, for a given central atom, the Sn-cage corresponds to the largest β_0^e; whereas, or a given metal cage atoms, the central atom Ni corresponds to the largest β_0^e. Due to this two combined effects, the endohedral all-metal electride cage $2e^{-}Mg^{2+}(Ni@Sn_{12})^{2-}Ca^{2+}$ exhibits the largest β_0^e value (16893 au) of the 9 all-metal electride studied. Furthermore, frequency-dependent $\beta^e(-2\omega;\ \omega,\ \omega)$ and $\beta^e(-\omega;\ \omega,\ 0)$ present the similar two atomic number effects of cage atoms and encapsulated central atom. The vibrational contribution to the largest longitudinal component to first hyperpolarizability (β_{xxx}^{nr}) of these nine all-metal electrides has also been studied. The nuclear relaxation contribution to the static first hyperpolarizability

is for seven of the nine all-metal electrides investigated larger than their electronic counterpart. For the particular case of $2e^{-}Mg^{2+}(Pt@Ge_{12})^{2-}Ca^{2+}$, the β_{xxx}^{nr} value of about 10^5 au, which is about 9 time of corresponding β_{xxx}^{e} value. Therefore, the vibrational contribution should be considered in the design of new NLO all-metal electrides.

Corresponding Authors

*E-mail: josepm.luis@udg.edu (Josep M. Luis)

*E-mail: wud@jlu.edu.cn (D. Wu).

*E-mail: lzr@jlu.edu.cn (Z.-R. Li).

Conflicts of interest

There are no conflicts to declare.

Acknowledgements

This study was supported by the National Natural Science Foundation of China (Grant No. 21573089, 21603032), the Graduate Innovation Fund of Jilin University (Grant No. 2017011), the Spanish Ministerio de Economıa y competividad (MINECO, CTQ2014-52525-P), and the Generalitat de Catalunya (project number 2014SGR931).

References

1 J. Zyss, *Molecular nonlinear optics: materials, physics, and devices*, Academic press, **2013**.
2 D. Burland, *Chem. Rev.*, 1994, **94**, 1-2.
3 D. M. Burland, R. D. Miller, C. A. Walsh, *Chem. Rev.*, 1994, **94**, 31-75.
4 K. Singh, J. R. Long, P. Stavropoulos, *J. Am. Chem. Soc.*, 1997, **119**, 2942-2943.
5 S. S. Hayat, M. A. Ortigoza, M. A. Choudhry, T. S. Rahman, *Phys. Rev. B*, 2010, **82**, 085405.
6 S. Muhammad, H. Xu, Y. Liao, Y. Kan, Z. Su, *J. Am. Chem. Soc.*, 2009, **131**, 11833-11840.
7 P. C. Ray, *Chem. Rev.*, 2010, **110**, 5332-5365.
8 F. Meyers, S. R. Marder, B. M. Pierce, J. L. Bredas, *J. Am. Chem. Soc.*, 1994, **116**, 10703-10714.
9 M. Nakano, H. Fujita, M. Takahata, K. Yamaguchi, *J. Am. Chem. Soc.*, 2002, **124**, 9648-9655.
10 J.-S. Yang, K.-L. Liau, C.-Y. Li, M.-Y. Chen, *J. Am. Chem. Soc.*, 2007, **129**, 13183-13192.
11 B. Kirtman, B. Champagne, D. M. Bishop, *J. Am. Chem. Soc.*, 2000, **122**, 8007-8012.
12 J. L. Dye, *Accounts chem. Res.*, 2009, **42**, 1564-1572.
13 W. Chen, Z. R. Li, D. Wu, F. L. Gu, X. Y. Hao, B. Q. Wang, R. J. Li, C. C. Sun, *J. Chem. Phys.*, 2004, **121**, 10489-10494.

14 Y. Li, Z. R. Li, D. Wu, R. Y. Li, X. Y. Hao, C. C. Sun, *J. Phys. Chem. B*, 2004, **108**, 3145-3148.
15 W. Chen, Z. R. Li, D. Wu, Y. Li, C. C. Sun, F. L. Gu, *J. Am. Chem. Soc.*, 2005, **127**, 10977-10981.
16 H. L. Xu, Z. R. Li, D. Wu, B. Q. Wang, Y. Li, F. L. Gu, Y. Aoki, *J. Am. Chem. Soc.*, 2007, **129**, 2967-2970.
17 J.-J. Wang, Z.-J. Zhou, Y. Bai, Z.-B. Liu, Y. Li, D. Wu, W. Chen, Z.-R. Li, C.-C. Sun, *J.Mater.Chem.*, 2012, **22**, 9652-9657.
18 Y. Bai, Z.-J. Zhou, J.-J. Wang, Y. Li, D. Wu, W. Chen, Z.-R. Li, C.-C. Sun, *J. Phys. Chem. A*, 2013, **117**, 2835-2843.
19 H.-L. Xu, Z.-R. Li, D. Wu, F. Ma, Z.-J. Li, F. L. Gu, *J. Phys. Chem. C*, 2009, **113**, 4984-4986.
20 H.-L. Xu, S.-L. Sun, S. Muhammad, Z.-M. Su, *Theor. Chem. Acc.*, 2010, **128**, 241-248.
21 R.-L. Zhong, H.-L. Xu, Z.-R. Li, Z.-M. Su, *J. Phys. Chem. Lett.*, 2015, **6**, 612-619.
22 H.-M. He, Z.-R. Li, Y. Li, W.-M. Sun, J.-J. Wang, J.-y. Liu, D. Wu, *J. Phys. Chem. C*, 2014, **118**, 23937-23945.
23 V. Postils, M. Garcia-Borras, M. Sola, J. M. Luis, E. Matito, *Chem. Commun. (Camb.)*, 2015, **51**, 4865-4868.
24 H.-M. He, Y. Li, W.-M. Sun, J.-J. Wang, D. Wu, R.-L. Zhong, Z.-J. Zhou, Z.-R. Li, *Dalton Trans.*, 2016, **45**, 2656-2665.
25 C. B. Benda, M. Waibel, T. F. Fässler, *Angew. Chem. Int. Edit.*, 2015, **54**, 365-365.
26 C. B. Benda, M. Waibel, T. F. Fässler, *Angew. Chem. Int. Edit.*, 2015, **54**, 522-526.
27 M. M. Bentlohner, W. Klein, Z. H. Fard, L. A. Jantke, T. F. Fässler, *Angew. Chem.*, 2015, **127**, 3819-3824.
28 N. Kazem, W. Xie, S. Ohno, A. Zevalkink, G. J. Miller, G. J. Snyder, S. M. Kauzlarich, *Chem. Mater.*, 2014, **26**, 1393-1403.
29 C. Lee, M. H. Whangbo, J. Köhler, *Anorg. Allg. Chem.*, 2010, **636**, 36-40.
30 H.-M. He, Y. Li, H. Yang, D. Yu, S.-Y. Li, D. Wu, J.-H. Hou, R.-L. Zhong, Z.-J. Zhou, F.-L. Gu, J. M. Luis, Z.-R. Li, *J. Phys. Chem. C*, 2017, **121**, 958-968.
31 H.-M. He, Y. Li, H. Yang, D. Yu, D. Wu, R.-L. Zhong, Z.-J. Zhou, Z.-R. Li, *J. Phys. Chem. C*, 2017, **121**, 25531-25540.
32 E. N. Esenturk, J. Fettinger, B. Eichhorn, *J. Am. Chem. Soc.*, 2006, **128**, 9178-9186.
33 P. Karamanis, *Int. J. Quantum Chem.*, 2012, **112**, 2115-2125.
34 G. Maroulis, *Chem. Phys.*, 2003, **291**, 81-95.
35 P. Karamanis, G. Maroulis, *Chem. Phys. Lett.*, 2003, **376**, 403-410.
36 G. Maroulis, *J. Chem. Phys.*, 1999, **111**, 583-591.
37 G. Maroulis, *Chem. Phys. Lett.*, 1996, **259**, 654-660.
38 G. Maroulis, *Chem. Phys. Lett.*, 1994, **226**, 420-426.
39 I. W. Bulik, R. Zalesny, W. Bartkowiak, J. M. Luis, B. Kirtman, G. E. Scuseria, A. Avramopoulos, H. Reis, M. G. Papadopoulos, *J. Comput. Chem.*, 2013, **34**, 1775-1784.
40 T. Yanai, D. P. Tew, N. C. Handy, *Chem. Phys. Lett.*, 2004, **393**, 51-57.
41 Y. Tawada, T. Tsuneda, S. Yanagisawa, T. Yanai, K. Hirao, *J. Chem. Phys.*, 2004, **120**, 8425-8433.
42 J. A. Bilbrey, A. H. Kazez, J. Locklin, W. D. Allen, *J. Comput. Chem.*, 2013, **34**, 1189-1197.
43 W. R. Wadt, P. J. Hay, *J. Chem. Phys.*, 1985, **82**, 284-298.

44 P. J. Hay, W. R. Wadt, *J. Chem. Phys.*, 1985, **82**, 270-283.
45 P. J. Hay, W. R. Wadt, *J. Chem. Phys.*, 1985, **82**, 299-310.
46 J. M. Luis, M. Duran, J. L. Andrés, B. t. Champagne, B. Kirtman, *J. Chem. Phys.*, 1999, **111**, 875-884.
47 C. Eckart, *Phys. Rev.*, 1926, **28**, 711-726.
48 P. J. Davis, P. Rabinowitz, In *Numerical Integration*; Blaisdell: London, 1967; pp 166−173.
49 D. M. Bishop, M. Hasan, B. Kirtman, *J. Chem. Phys.*, 1995, **103**, 4157-4159.
50 J. M. Luis, J. Martí, M. Duran, J. L. Andrés, B. Kirtman, *J. Chem. Phys.*, 1998, **108**, 4123-4130.
51 C. E. Dykstra, P. G. Jasien, *Chem. Phys. Lett.*, 1984, **109**, 388-393.
52 P. Pulay, *J. Chem. Phys.*, 1983, **78**, 5043-5051.
53 Z.-J. Li, Z.-R. Li, F.-F. Wang, C. Luo, F. Ma, D. Wu, Q. Wang, X.-R. Huang, *J. Phys.Chem. A*, 2009, **113**, 2961-2966.
54 M. J. Frisch, G. W. Trucks, H. B. Schlegel, G. E. Scuseria, M. A. Robb, J. R. Cheeseman, G. Scalmani, V. Barone, B. Mennucci, G. A. Petersson, H. Nakatsuji, M. Caricato, X. Li, H. P. Hratchian, A. F. Izmaylov, J. Bloino, G. Zheng, J. L. Sonnenberg, M. Hada, M. Ehara, K. Toyota, R. Fukuda, J. Hasegawa, M. Ishida, T. Nakajima, Y. Honda, O. Kitao, H. Nakai, T. Vreven, J. A. Montgomery, Jr., J. E. Peralta, F. Ogliaro, M. Bearpark, J. J. Heyd, E. Brothers, K. N. Kudin, V. N. Staroverov, R. Kobayashi, J. Normand, K. Raghavachari, A. Rendell, J. C. Burant, S. S. Iyengar, J. Tomasi, M. Cossi, N. Rega, J. M. Millam, M. Klene, J. E. Knox, J. B. Cross, V. Bakken, C. Adamo, J. Jaramillo, R. Gomperts, R. E. Stratmann, O. Yazyev, A. J. Austin, R. Cammi, C. Pomelli, J. W. Ochterski, R. L. Martin, K. Morokuma, V. G. Zakrzewski, G. A. Voth, P. Salvador, J. J. Dannenberg, S. Dapprich, A. D. Daniels, O¨. Farkas, J. B. Foresman, J. V. Ortiz, J. Cioslowski and D. J. Fox, Gaussian 09 Revision E.01, Gaussian Inc., Wallingford CT, 2009.
55 R. Dennington, T. Keith, J. Millam, GaussView, Version 5; Semichem Inc.: Shawnee Mission, KS, 2009.
56 R.-L. Zhong, H.-L. Xu, S. Muhammad, J. Zhang, Z.-M. Su, *J. Mater. Chem.*, 2012, **22**, 2196-2202.
57 J.-J. Wang, Z.-J. Zhou, Y. Bai, H.-M. He, D. Wu, Y. Li, Z.-R. Li, H.-X. Zhang, *Dalton Trans.*, 2015, **44**, 4207-4214.
58 W. M. Sun, D. Wu, Y. Li, J. Y. Liu, H. M. He, Z. R. Li, *Phys. Chem. Chem. Phys.*, 2015, **17**, 4524-4532.
59 M. Niu, G. Yu, G. Yang, W. Chen, X. Zhao, X. Huang, *Inorg. Chem.*, 2014, **53**, 349-358.
60 B. Li, C. Xu, X. Xu, C. Zhu, F. L. Gu, *PCCP*, 2017, **19**, 23951-23959.
61 M. Garcia-Borras, M. Sola, J. M. Luis, B. Kirtman, *J. Chem. Theory Comput.*, 2012, **8**, 2688-2697.
62 H. Y. Wu, A. Chaudhari, S. L. Lee, *J. Comput. Chem.*, 2005, **26**, 1543-1564.

TOC Graphic

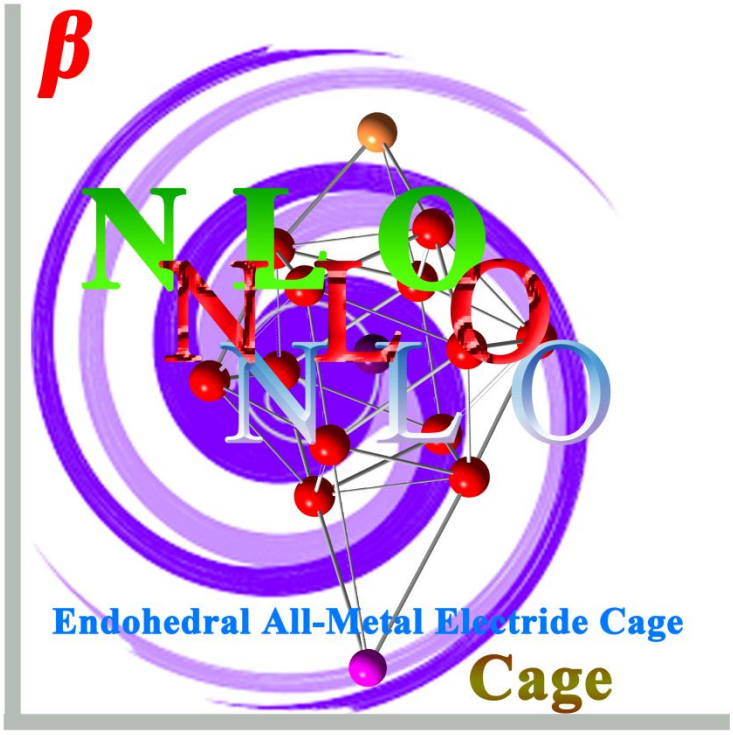

The endohedral all-metal electride cages $2e^{-}Mg^{2+}(M@E_{12})^{2-}Ca^{2+}$ (M = Ni, Pd, and Pt; E= Ge, Sn, and Pb) exhibit the better NLO response.